Green and Smart Mining Engineering 1 (2024) 40–52

Contents lists available at ScienceDirect

Green and Smart Mining Engineering

journal homepage: www.keaipublishing.com/en/journals/gsme

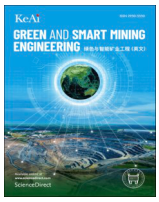

Review of allanite: Properties, occurrence and mineral processing technologies

Zhongqing Xiao, Wencai Zhang*

Department of Mining and Minerals Engineering, Virginia Tech, Blacksburg, VA 24061, USA

ARTICLE INFO

Keywords:
Allanite
Rare-earth elements
Radiation damage
Occurrence
Processing technologies

ABSTRACT

Allanite is commonly encountered as an accessory rare-earth silicate mineral in association with minerals such as garnet, biotite, and feldspar. It is distributed globally and occurs in igneous formations such as granites, pegmatites, and syenites, as well as in various metamorphic rocks such as schist, gneiss, and amphibolite. Moreover, it can be found in mineral veins formed through hydrothermal activity. While allanite has not yet been extensively utilized for the production of rare-earth elements, recent discoveries of high-grade rare-earth-rich allanite deposits in Wyoming, USA, highlight its economic potential. However, despite ongoing research on the mineralogy and processing of rare-earth minerals, allanite has not received widespread attention in mineral processing. To achieve economical extraction of rare-earth elements from allanite in the future, systematic studies on processing techniques (e.g., density separation, magnetic separation, flotation, leaching) are imperative to fully unlock the potential of allanite as a rare-earth element source. To pave the way for future investigation of allanite and address the unique processing challenges, this review article aims to comprehensively summarize previous studies, encompassing properties, occurrences, and processing technologies of allanite.

1. Introduction

As shown in Table 1, rare-earth elements (REEs) are a set of 17 chemical elements found in the periodic table, including yttrium and scandium, and 15 metallic elements from the lanthanide series. Based on atomic number, REEs from lanthanum to europium are typically classified as light REEs (LREEs), while those from gadolinium to lutetium, including yttrium, fall into the category of heavy REEs (HREEs) [1]. Despite the presence of "rare" in their name, some REEs are relatively abundant in Earth's crust, comparable to industrial metals and significantly higher than precious metals. For example, the crustal abundance of cerium stands at approximately 63 ppm, while copper, silver, and gold have crustal abundances of 60, 0.075, and 0.004 ppm, respectively [2–5]. The term "rare" primarily indicates that REEs are widely dispersed and infrequently found in concentrated and economical ore deposits [6,7].

As shown in Table 2, more than 250 distinct species of rare-earth minerals (REMs) have been described, which can be grouped as halides, carbonates, oxides, phosphates, and silicates [8–11]. REMs are defined by their chemical composition rather than the content of REEs in the minerals. Numerous REMs contain relatively low concentrations of REEs, typically in the range of 10–300 ppm [8,12,13]. Nevertheless, presently extracted rare-earth ore grades exhibit an average of 5% REEs, with some reaching as high as 15% [14,15].

In primary deposits, the three rare-earth-bearing minerals of significant commercial interest that are commonly extracted are bastnaesite, xenotime, and monazite [16–18]. Bastnaesite is a fluorocarbonate mineral with an approximate composition of 70% rare-earth oxides (REOs), primarily consisting of cerium, lanthanum, praseodymium, and neodymium [12]. Bastnaesite is the most abundant REM, contributing to roughly 80% of the world's total REE production. This prevalence is attributed to its abundant presence in ore deposits such as Mountain Pass, California, and Bayan Obo, China [19,20]. Monazite is a phosphate mineral with an approximate 70% REO composition, primarily comprising cerium, lanthanum, praseodymium, and neodymium. Moreover, monazite contains 4%–12% thorium and varying amounts of uranium. This mineral is commonly found in placer deposits and beach sands and is also a component of the Bayan Obo deposit [12,21,22]. Xenotime, often found in association with monazite, is an yttrium phosphate mineral with an approximate 67% REO

Peer review under the responsibility of Editorial Board of Green and Smart Mining Engineering.
* Corresponding author.
E-mail address: wencaizhang@vt.edu (W. Zhang).

https://doi.org/10.1016/j.gsme.2024.04.004
Received 2 March 2024; Received in revised form 22 March 2024; Accepted 27 March 2024
Available online 5 April 2024

Table 1
Description of rare-earth elements (REEs).

Classification	REE	Symbol	Atomic number [30]	Oxidation state [12]	Trivalent ionic radius (Å, coordination number VIII) [31,32]	Abundance in the upper crust (ppm) [1,4,5]
Light REEs	Lanthanum	La	57	+ 3	1.16	31
	Cerium	Ce	58	+ 3/+ 4	1.14	63
	Praseodymium	Pr	59	+ 3	1.13	7.1
	Neodymium	Nd	60	+ 3	1.11	27
	Promethium	Pm	61	+ 3	1.09	*
	Samarium	Sm	62	+ 2/+ 3	1.08	4.7
	Europium	Eu	63	+ 2/+ 3	1.07	1
Heavy REEs	Gadolinium	Gd	64	+ 3	1.05	4
	Terbium	Tb	65	+ 3	1.04	0.7
	Dysprosium	Dy	66	+ 3	1.03	3.9
	Holmium	Ho	67	+ 3	1.02	0.83
	Erbium	Er	68	+ 3	1.00	2.3
	Thulium	Tm	69	+ 2/+ 3	0.99	0.3
	Ytterbium	Yb	70	+ 2/+ 3	0.99	2.2
	Lutetium	Lu	71	+ 3	0.98	0.31
	Yttrium	Y	39	+ 3	1.02	21
	Scandium	Sc	21	+ 3	0.87	14

* Promethium does not occur naturally.

Table 2
Classification of rare-earth minerals. Reproduced with permission from Ref. [16]. Copyright (2006) Elsevier.

Mineral class		Mineral examples and chemical formula
Halides		Fluocerite-(F), CeF_3
Carbonates	With fluoride	Bastnaesite, $(Ce,La)(CO_3)F$
	Without fluoride	Ancylite, $(Ce,Sr,Ca)(CO_3)(OH,H_2O)$
Borates		Braistschite, $(Ca,Na_2)_7CeB_{22}O_{43}{\cdot}7\ H_2O$
Oxides and hydrates	AO_2 type	Cerianite, $(Ce^{4+},Th^{4+})O_2$
	ABO_3 type	Perovskite group, $(Ca,Ce,Na,Sr)(Ti,Nb,Ta)O_3$
	ABO_4 type	Fergusonite–formanite, $Y(Nb,Ta)O_4$–$Y(Ta,\ Nb)O_4$
	$AB_2(O,OH)_6$ type	Euxenite group, $(Y,Ca,Ce,U,Th)(Nb,Ta,Ti)_2O_6$
	$A_2B_2O_6(O,OH,F)$ type	Pyrochlore group, $(Na,RE,K,U)_2(Nb,Ta,Ti)_2(O,OH,F)$
	Others	Hibonite, $(Ca,Ce)(Al,Ti,Mg)_{12}O_{19}$
Phosphates, arsenates, and vanadates		Apatite, $(Ca,RE,Sr,Na,K)_3Ca_2(PO_4)_3(F,OH)$
		Monazite, $(Ce,La)PO_4$
		Xenotime, YPO_4
Silicates	Isolated group	Cerite, $(Ce,La,Ca)_9(Fe^{3+},Mg)(SiO_4)_6[SiO_3(OH)](OH)_3$
		Garnet, $(Ca,Fe,Mg,Mn,Y)_3(Al,Cr,Fe,Mn,Ti,V,Zr)_2(Si,Al)_3O_{12}$
		Sphene, $CaTiSiO_4$
	Diortho group	Allanite, $Ca(Ce,Y,Ca)Al(Al,Fe)(Fe,Al)(SiO_4)_3(OH)$
	Chain group	Stillwellite, $CeBSiO_5$
	Ring group	Eudialyte, $(Na,Ca,Ce)_6(Zr,Fe)_2Si_7(O,OH,Cl)_{22}$
	Sheet group	Gadolinite, $(Y,Ce)_2Fe^{2+}Be_2Si_2O_{10}$
	Framework group	Kainosite, $Ca_2(Y,RE)_2(Si_4O_{12})CO_3{\cdot}H_2O$
	Others	Iimoriite, $Y_2(SiO_4)(CO_3)$

composition. However, it contains significantly lower amounts of cerium, lanthanum, praseodymium, and neodymium than monazite and bastnaesite [12,23–25]. Furthermore, ion adsorption clay deposits, notably in China, are significant secondary sources of REEs [7]. While the REE content in ion adsorption REE deposits is relatively modest, ranging from 0.05wt% to 0.3wt%, their exploration is relatively straightforward and cost-effective [26]. Notably, these deposits are comparatively abundant in HREEs and contribute to over 90% of the world's HREE production [27–29].

REEs have unique physical, chemical, mechanical, electronic, magnetic, luminescence, phosphorescence, and catalytic properties [15,33]. REEs have earned the moniker of "the vitamins of the modern industry" due to their role in significantly enhancing efficiency, reliability, and durability [1,33]. Moreover, viable substitutes for REEs are either inferior or yet to be identified [13]. The demand for REEs is steadily on the rise, driven by their increasing utilization in various emerging technological applications, particularly their pivotal role in the industrial transition to a green economy and their essential contribution to the production of numerous carbon-neutral technologies [1,15,34].

However, the declining availability of economically feasible rare-earth deposits coupled with a mixture of technological, economic, and geopolitical obstacles raises concerns about the scarcity of REEs and a potential global shortage [35]. To address the ever-increasing demand for REEs, current solutions include (1) developing technologies that can substitute REEs with less critical materials to reduce dependence on them, (2) investing in sustainable primary and secondary REE mining to ensure a more stable and environmentally responsible supply chain, and (3) developing sustainable REE recycling processes to recover and reuse REEs from various products, reducing the need for new mining operations [1,36–42].

Allanite, an REM found in certain existing rare-earth deposits, is a significant accessory mineral in various geological settings, including granites, pegmatites, high-pressure gneisses, garnet-amphibolites, and eclogites [43–48]. Although allanite has not been economically utilized for REE production, its economic potential in regions such as Australia, Asia, Turkey, Canada, the United States, and Europe has been reported [49]. Recently, American Rare Earths has made significant discoveries of new high-grade rare-earth deposits in Wyoming, USA, where REEs are concentrated in veins enriched with allanite [50]. While research on the mineralogy and processing of REMs has been ongoing for some

time, the primary focus has been on minerals such as bastnaesite, xenotime, monazite, and ion adsorption clays. Meanwhile, recent research has focused on extracting REEs from coal, coal byproducts, acid mine drainage, and other secondary feedstocks. Based on the available literature, the study of allanite has not received in-depth attention, especially concerning mineral processing. To pave the way for a systematic investigation of allanite in the future and address the unique processing challenges, this review article aims to comprehensively summarize previous studies, encompassing properties, occurrences, and processing technologies of allanite.

2. Methodology

To conduct a comprehensive screening and summary of allanite research articles, first, an extensive search is conducted across prominent databases such as ScienceDirect, Scopus, SpringerLink, Google Scholar, OneMine, and Web of Science using relevant keywords such as "allanite." Subsequently, the abstracts of the identified papers are meticulously reviewed. During this phase, papers are selected and categorized based on their pertinence to various aspects of allanite, including its properties, occurrences, and processing technologies. Following this, the chosen papers are thoroughly examined, with a keen focus on extracting and summarizing critical information. Concurrently, an exploration of relevant papers cited within the literature is undertaken to foster a deeper understanding of the subject matter. Finally, the gathered insights are synthesized to facilitate discussions concerning the current state of allanite research while delineating potential avenues for future exploration in this field.

As of the time of manuscript preparation, the Web of Science database has yielded a total of 211 publications related to "allanite" in their titles. Fig. 1(a) illustrates that despite the relatively small overall number of publications, there has been a discernible upward trend in the volume of articles dedicated to allanite research over the past two decades. These publications cover a range of research areas, with the top three being mineralogy, geochemistry and geophysics, and geology, constituting 38.0%, 30.5%, and 15.6% of the total, respectively, as shown in Fig. 1(b).

It is worth noting that only a mere fraction (3.2%) of the literature concerning allanite focused on mining and mineral processing, which suggests that there is a huge potential for research in this area. Specifically, there is currently a lack of dedicated research on the density and magnetic separation of allanite ore. Only two articles mentioned obtaining allanite sample through magnetic separation in laboratory settings for subsequent flotation studies. In most density and magnetic separation studies, allanite, considered a minor accessory REM, was enriched alongside other primary REMs. Furthermore, there are merely three papers dedicated to allanite flotation research and another three focusing on allanite leaching.

3. Properties and application

3.1. Formula, chemical substitutions, physical properties, and crystal structure

Allanite, named in honor of the Scottish mineralogist Thomas Allan (1777–1833), is a rare-earth silicate mineral within the epidote mineral group. In previous research, it was also referred to as "orthite," although this term is now considered obsolete [51,52]. Allanite is usually black to brownish-black in color and forms either thick tablets or structures resembling sticks or needles [51,53].

The general formula of allanite is $A_2M_3Si_3O_{12}$ [OH], with site A accommodating REEs, Ca, Sr, Pb, Mn, Th, and U and site M being Al, Fe, Mn, Mg, Ti, Cr, and V [25,51,54]. Moreover, in rare cases, Si may undergo partial substitution by P, Ge, or potentially Be [51]. Table 3 shows the elemental composition of allanite from selected studies. Gieré and Sorensen suggested that the total REE content of allanite typically falls within the range of 14wt% to 33wt%, with LREEs constituting more than 90% of the total [51]. Hence, allanite serves as a valuable source of REEs. The trend of REE composition within allanite follows Ce > La > Nd > > Pr > Sm > Gd [51,55,56]. Within the allanite group, the common species are classified based on the predominant REE present, including allanite-(Ce), allanite-(La), and allanite-(Y) [51,52,57,58].

Due to the similarity in ionic radius between REEs and heterovalent ions, substitutions involving REEs and ions such as Na^+, Ca^+, Th^{4+}, and U^{4+} are common in the mineral structure. Such isomeric substitutions primarily occur in oxides and silicates [16]. When represented by the chemical formula $CaREEAl_2Fe^{2+}Si_3O_{12}$ [OH], allanite exhibits coupled substitutions, as described in Eq. (1) with epidote and Eq. (2) with clinozoisite [51,59,60].

$$REE^{3+} + Fe^{2+} \leftrightarrow Ca^{2+} + Fe^{3+} \quad (1)$$

$$REE^{3+} + Fe^{2+} \leftrightarrow Ca^{2+} + Al^{3+} \quad (2)$$

The individual physical properties of allanite exhibit significant variation due to the mineral's highly variable composition and varying degrees of metamictization [51]. For instance, parameters of allanite such as refractive index, birefringence, and density increase with an increase in REE and Fe content [61,62].

Epidotes are categorized within the disilicate or sorosilicate structural family because they feature [SiO_4] tetrahedral units organized in pairs, with each pair connected by a shared oxygen atom [51,54,63,64]. The tetrahedral anionic group of allanite is arranged in a Diortho group

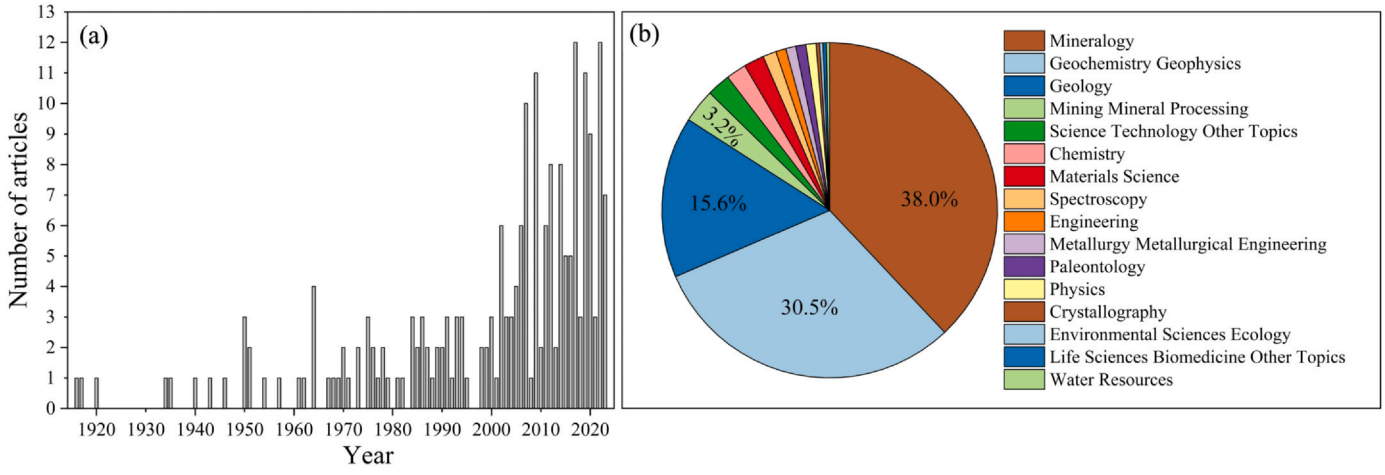

Fig. 1. Allanite articles categorized by (a) publication year and (b) research area (data from the Web of Science).

Table 3
Elemental content (wt%) in allanite from selected studies.

Reference	Si	Al	Fe	Mg	Ca	Na	K	Ti	P	Mn	Th	U
[79]	14.84	9.21	10.84	-	7.57	-	-	-	0.03	-	-	-
	15.37	9.87	10.90	-	9.46	-	-	-	-	-	0.09	-
	15.25	9.81	10.10	-	8.79	-	-	-	0.04	-	-	-
	16.17	10.63	10.01	-	11.35	-	-	0.08	-	-	-	-
	16.27	10.79	10.15	-	11.81	-	-	0.05	-	-	-	-
[70]	16.79	4.64	3.67	-	3.32	-	0.81	-	-	-	2.18	0.81
	23.23	13.04	7.41	-	3.20	-	2.10	-	-	-	2.78	1.09
	12.94	6.12	3.27	-	6.50	-	1.41	-	-	-	0.64	0.46
	18.27	9.39	5.73	-	3.25	-	3.01	-	-	-	1.67	0.86
	14.55	4.95	4.06	-	3.24	1.99	1.14	11.70	-	-	2.51	1.16
	10.15	3.03	3.31	-	3.98	1.79	0.98	14.60	-	-	2.52	1.13
[48]	15.29	8.46	11.76	0.37	7.58	-	-	0.13	0.03	0.62	1.00	0.07
[73]	14.86	7.57	9.94	1.13	7.82	-	-	0.56	-	0.24	0.48	-
	14.82	8.02	9.42	-	-	0.10	-	-	-	0.30	1.04	-
	14.83	7.11	12.74	-	-	-	-	-	-	2.10	1.40	-
[80]	15.55	9.56	7.15	0.17	5.37	0.15	0.02	0.25	0.01	0.99	0.58	-

La	Ce	Pr	Nd	Sm	Eu	Gd	Tb	Dy	Ho	Er	Tm	Yb	Lu	Y	Sc
5.28	10.45	1.15	4.42	0.78	-	0.74	-	-	-	-	-	-	-	-	-
3.79	7.82	0.93	3.35	0.62	-	0.84	-	-	0.05	-	-	-	-	0.09	-
4.15	8.74	0.97	3.82	0.70	-	0.87	-	-	0.09	-	-	-	-	-	-
2.63	5.32	0.68	2.28	0.47	-	0.95	-	-	-	-	-	-	-	-	-
2.42	5.02	0.62	2.14	0.35	-	0.89	-	-	-	-	-	-	-	-	-
18.73	32.16	2.28	8.29	0.24	0.26	1.27	-	-	-	-	-	-	-	4.20	-
9.35	21.62	2.51	7.41	0.51	0.31	1.12	-	-	-	-	-	-	-	4.03	-
18.67	33.32	2.26	7.06	-	0.56	1.71	-	-	-	-	-	-	-	4.69	-
15.28	26.09	2.25	6.76	-	-	0.51	-	-	-	-	-	-	-	6.47	-
12.91	22.60	1.30	7.66	1.52	0.27	0.82	-	-	-	-	-	-	-	4.99	-
12.62	24.61	2.40	7.23	1.36	0.32	1.17	-	-	-	-	-	-	-	5.00	-
3.97	7.03	0.66	3.94	0.68	0.02	0.45	-	-	0.15	-	0.04	0.07	0.12	0.18	0.02
5.97	9.79	0.60	2.47	-	-	-	-	-	-	-	-	-	-	-	-
2.24	6.03	0.93	4.26	1.49	-	1.03	0.10	0.25	-	-	-	-	-	1.02	0.20
4.89	8.86	0.74	1.89	-	-	-	-	-	-	-	-	-	-	-	0.12
2.90	9.17	1.13	4.59	0.76	-	0.45	-	0.09	0.15	-	-	-	-	0.72	-

-: The number is either too negligible to be considered or remains unreported.

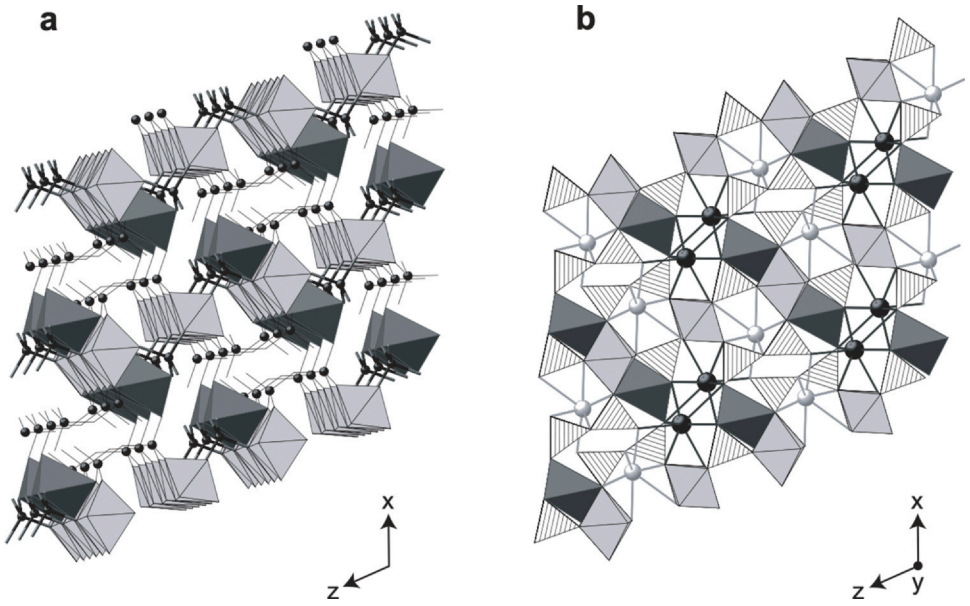

Fig. 2. Crystal structure of allanite consisting of chains of edge-sharing octahedra parallel to "010": M(1) and M(2) sites are light gray octahedra; M(3) octahedra are shown as dark octahedra. These chains are linked by single SiO_4 tetrahedra and double-tetrahedral groups (Si_2O_7). (a) Simplified diagram showing M and T sites only, viewed slightly off the *b* axis. (b) View parallel to the *b* axis [51]. Reproduced with permission from Ref. [51]. Copyright (2004) Mineralogical Society of America.

manner [16,51]. The crystal structure of allanite, depicted in Fig. 2, contains two sets of chains composed of edge-sharing octahedra (M sites) aligned parallel to "010". These chains are interlinked through two types of tetrahedral (T) sites, which include isolated SiO_4 tetrahedra and corner-sharing pairs of tetrahedral groups (Si_2O_7). For a more comprehensive description of the structure, readers are referred to Gieré and Sorensen's research [51].

3.2. Radioactive elements and rock dating

Allanite often exhibits enrichment in thorium and uranium due to the similarity in the outer electron shell structures of Th, U, and REE, facilitating their isomorphism within minerals. Moreover, thorianite and uranothorianite have also been identified to coexist with allanite as separate minerals [53]. ThO_2 content in allanite varies from 2wt% to

3wt%, occasionally reaching levels as high as 4.9wt%. Conversely, the concentration of U is typically lower than that of Th, generally falling within the <1000 ppm range [51,65].

Given its capacity to incorporate Th and U into its lattice structure, coupled with its formation under a broad spectrum of metamorphic and magmatic conditions, allanite emerges as a valuable geochronological tool for constraining geological events [66,67]. Vazquez and Reid [68] employed a combination of *in situ* compositional and isotopic analyses on allanite to date and quantify compositional zoning within and between crystals using ^{238}U–^{230}Th disequilibrium methods, achieving an age resolution of tens of thousands of years. Burnham *et al.* [69] conducted allanite geochronology studies for four mineral deposits in Mount Isa Inlier, namely, SWAN, Mary Kathleen, Koppany, and Elaine Dorothy. Their data reveal the presence of multiple phases of allanite formation, including one at 1732 ± 8 Ma at Koppany, another at approximately 1520 Ma at Mary Kathleen, Koppany, and SWAN, and a third at around 1473 Ma at Mary Kathleen and Elaine Dorothy, associated with vein calcite. These findings provide valuable insights into the geological history and mineralization processes in Mount Isa Inlier. In ultrahigh-pressure metamorphic rocks found in the Dabie–Sulu orogen of central-east China, allanite within the Jingshan granite has formed in response to the subduction and remelting of Dabie–Sulu gneiss. Allanite records the ages of Triassic ultrahigh-pressure metamorphism and Jurassic peritectic-magmatic events, contributing to the understanding of the evolution of the Dabie–Sulu orogen [66].

3.3. Radiation damage and thermal annealing

Excessive levels of radioactive elements in ores can have negative impacts on both mineral processing difficulty and human health. Abdel Gawad *et al.* [70] assessed the radioactive risk associated with syenogranite and quartz syenite in the Wadi Rod Elsayalla area. These rocks are enriched in radioactive minerals, including allanite, uranothorite, monazite, zircon, and yttrocolumbite. The mean activity concentrations of ^{238}U, ^{232}Th, and ^{10}K were measured to be 62.2 ± 20.8, 84.2 ± 23.3, and 949.4 ± 172.5 $Bq{\cdot}kg^{-1}$, respectively, surpassing the recommended limits.

Moreover, in Fig. 3, minerals containing radioactive elements often exhibit signs of radiation damage, undergoing a partial or complete transformation into defect-rich crystalline structures and radiation-amorphized nanoregions [52,71–74]. The radiation damage is primarily caused by the displacement of atoms within their crystal structure due to the impact of recoil nuclei. The extent of this damage depends on the radiation dose, altering allanite's physical properties [51]. Notably, the more altered sections of allanite display lower radioactivity than the unaltered portions. It was suggested that uranium and thorium have a higher migration capacity relative to REEs, potentially leading to the leaching of radioactive elements during the alteration process [51,53]. Meanwhile, the presence of microcracks in metamorphic materials increases the surface area of the allanite grains, and the disordered state enhances its susceptibility to chemical alteration and solubility in acids. Therefore, metamict allanite is more susceptible to leaching or dissolution [51,74–76].

Thermal annealing of metamict allanite results in partial recrystallization and recovery of the structure [77]. Reissner *et al.* [78] found that radiation-damaged allanite-(Ce) begins to recrystallize at an annealing temperature below 700 K. Moreover, oxidation of Fe^{2+} to Fe^{3+} and dehydration occur during this process. Gatta *et al.* [48] investigated the thermal behavior of a natural allanite-(Ce) up to 1073 K at ambient pressure. They found that allanite exhibits ideal elastic behavior up to 700 K, but its behavior deviates from the elasticity field at temperatures between 700 and 800 K. Despite this deviation, allanite maintains its crystallinity up to 1073 K. Beirau *et al.* [77] noted that when heating allanite to 1273 K in air, its crystal structure was destroyed.

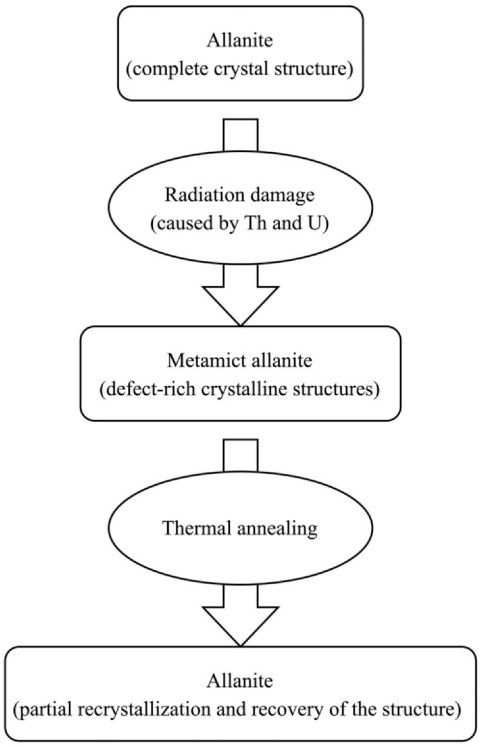

Fig. 3. Effects of radiation damage and thermal annealing processes on the crystallinity and crystal structure of allanite.

4. Occurrence and geological context

Allanite is commonly encountered as an accessory mineral in association with minerals such as garnet, biotite, and feldspar. It is distributed globally and occurs in igneous formations such as granites, pegmatites, and syenites, as well as in various metamorphic rocks such as schist, gneiss, and amphibolite. Moreover, it can be found in mineral veins formed through hydrothermal activity [51,56,81–86]. Allanite in ores can manifest as disseminated crystals, exhibiting either zonal or finely zoned characteristics, as well as veins of varying widths, ranging from several millimeters to several meters [53,87].

The formation and occurrence of allanite are intimately connected to geological processes such as metamorphism, igneous activity, and hydrothermal alteration. The appearance and texture of allanite can vary significantly depending on the specific metamorphic reactions it has undergone during the metamorphic process [46,88–90]. Airaghi *et al.* [91] examined metapelites from the central Longmen Shan and identified whole rock composition and fluid availability during metamorphism as probable factors that contribute to textural variations among allanite samples. Allanite-(Ce) in the granites of the aluminous association in Graciosa Province, southern Brazil, exhibits intricate zoning patterns. Primary allanite undergoes variable postmagmatic transformations due to interactions with a fluid phase and metamictization induced by radioactive decay [92]. Akhila *et al.* [93] analyzed allanite formed approximately 1.8 billion years ago in the multimetallic mineralized domain of the Singhbhum shear zone. Optical and textural variations in allanite suggest not only multigenerational processes in its formation but also significant changes in hydrothermal properties.

The process of allanite formation is closely related to monazite. In the peraluminous biotite granodiorite-tonalite found in the Tribeč Mountains, monazite often contains polymineralic inclusions dominated by anhedral allanite [94]. Petrological investigations have revealed that allanite often forms as a result of the alteration of detrital, metamorphic monazite [89,90,95]. In contrast, allanite is consumed during the staurolite-in reaction, leading to the formation of monazite [89,96,97]. Cavallo and Dino [98] examined waste materials from

gneiss (Beola and Serizzo from Piedmont, northern Italy), proposing that the formation of allanite involves the transformation of igneous iron-rich biotite into a more magnesium-rich variant. Subsequently, the released Fe^{2+} reacts with monazite and clinozoisite.

When allanite undergoes weathering, it can lead to ion adsorption rare-earth deposits. Zhao *et al.* [99] investigated the allanite in the bedrock of the extensive Bachi ion adsorption LREE deposit in South China. Allanite hosts a significant portion, at least 80%, of the LREEs in the deposit. Structural and geochemical alterations from primary allanite to altered allanite facilitate its weathering, and the weathering of synchysite-(Ce) releases LREE ions, contributing to the formation of ion adsorption LREE deposits.

It is worth mentioning that in the Kingman pegmatite situated in the Cerbat Range of northwestern Arizona, allanite-(Nd), distinguished by its prevalence of neodymium, was discovered. The allanite-(Nd) often found near grain rims and along fractures may result from alteration by highly oxidizing late-stage fluids. These fluids could have preferentially redistributed Ce into bastnasite-(Ce), thereby leading to the formation of Nd-enriched recrystallized allanite along fractures and rims [100].

5. Processing technologies

In the industrial processing of rare-earth ores, a combination of methods such as density separation, magnetic separation, electrostatic separation, flotation, sulfuric acid roasting, leaching, and solvent extraction is commonly employed [12,25,101–104]. Currently, there is a scarcity of research on the mineral processing of allanite ore. Only three studies have focused on the flotation of allanite, and another three studies have examined the direct leaching of allanite. In particular, only two allanite flotation papers provide detailed descriptions of the magnetic separation research of allanite samples. In most density and magnetic separation studies, allanite, considered a minor accessory REM, was enriched alongside other primary REMs. Consequently, an additional section discussing the outcomes of density and magnetic separation used for complex REMs containing allanite was added to the density and magnetic separation section by the authors.

5.1. Density and magnetic separation

Due to metal minerals such as allanite typically possessing relatively high specific gravities (SGs), density separation is commonly effective in eliminating low-specific-density gangue minerals such as quartz. Meanwhile, in magnetic separation, low-intensity magnetic separators are employed to remove ferromagnetic gangue minerals such as magnetite, while high-intensity magnetic separators (HIMSs) are utilized to concentrate paramagnetic minerals such as allanite [8,54,98,105].

5.1.1. Complex REMs containing allanite

Karan *et al.* [106] performed sink-float analysis using heavy media liquids with SGs of 2.84 and 3.32 on the rare-earth ores located in Bhatikheda, Siwana Ring Complex, Rajasthan, India. The coarsely ground feed (0.5 mm) contained allanite, zircon, gittinsite, and traces of monazite, with major gangue minerals including aegirine and K-feldspar. The results revealed that coarse-grained allanite (180–450 μm) was segregated in the fraction with SG > 3.32, while comparatively finer-sized allanite was found in the fraction with SG < 3.32, accompanied by quartz and K-feldspar. Given the considerable variability in the occurrence of REE phases within the ore, spanning from fully liberated grains to finely disseminated ones within lighter gangue minerals, density separation yielded limited results.

Stouraiti *et al.* [107] investigated the beneficiation of rare-earth ores sourced from heavy mineral sands of Nea Peramos, Kavala, Northern Greece, through particle size classification coupled with HIMS. The ore feed size ranged from 1.70 to 0.150 mm and comprised diamagnetic minerals (e.g., albite, quartz, K-feldspar), paramagnetic minerals (e.g., titanite, Mg-hornblende, allanite), and ferromagnetic minerals (e.g., hematite, magnetite). Both dry HIMS (DHIMS) and wet HIMS (WHIMS) were applied separately to concentrate REMs. In DHIMS, a magnetic field of 2 T was employed, with conveyor tilts set to 72°, 74°, and 76° individually. The results demonstrated significant improvements in REE recovery when applied to each particle size separately, achieving recoveries of 88%–92%. Comparable REE recoveries were attained by processing the undersize 0.50 mm, i.e., 79%–96%. The actual total REE (TREE) concentration in the magnetic products was 2.8 times higher than the initial feed contents. In WHIMS, two different magnetic fields (i.e., 0.48 and 2.4 T) were applied. The final cumulative magnetic concentrate exhibited a 2.5-fold increase in allanite content, from 3wt% in the initial composite feed to 8wt% in the magnetic concentrate. Moreover, the REE contents of the final magnetic concentrates increased by a factor of 2.8 compared with those of the initial feed. However, the high thorium content, following the enrichment trend of LREEs in the concentrates, constrained the concentration process.

Raslan *et al.* [105] investigated the utilization of HIMS combined with density preconcentration steps via a shaking table concentrator to recover REMs from the Wadi el-Sheikh pegmatitic granitoid sample in the Central Eastern Desert of Egypt. The process involved an ore sample size of 1 mm to 45 μm, with d_{80} and d_{50} of the ore measuring 900 and 500 μm, respectively. Using a heavy liquid with an SG of 2.89, the light fractions (SG < 2.89) predominantly comprised quartz and feldspar, while the heavy fractions (SG > 2.89) primarily consisted of euxenite-(Y), fergusonite-(Y), allanite-(Ce), xenotime-(Y), uranothorite, zircon, and magnetite. Subsequently, three magnetic field currents (i.e., 0.1, 1.5, 3.0 A) were applied in the magnetic separation step, wherein euxenite-(Y), fergusonite-(Y), xenotime-(Y), and allanite-(Ce) were identified as the strong paramagnetic minerals that separated at 1.5 A. The final magnetic concentrate contained up to 63.63wt% heavy minerals, with a final recovery of 78.2%, representing a mass of 8.55% out of the original sample assays, which contained 7.59wt% heavy minerals.

5.1.2. Allanite samples

To prepare allanite samples for flotation or leaching studies, two studies mentioned specialized purification of allanite through magnetic separation techniques. The allanite sample studied by Jordens *et al.* [8] comprised 64.8wt% allanite. The major minerals exhibited magnetic properties such as paramagnetic (allanite, ankerite, fluorite), diamagnetic (quartz, calcite, pyrite), and ferro/paramagnetic (iron oxides, other silicates). The fractions of the allanite sample ranging from 106 to 25 μm were treated separately at approximately 2.1 and 0.45 T to remove the less magnetic and strongly magnetic fractions, respectively. The X-ray diffraction (XRD) results showed that the primary peak of the purified allanite sample corresponded perfectly with all available allanite patterns.

Kursun *et al.* [25] purified an allanite sample from the Mary Kathleen reserve in Queensland, Australia, through magnetic separation. The sample was crushed with a mortar and pestle and then dry-sieved to obtain fractions of 500 to 212 μm. A dry HIMS under 1.66 T was used to remove nonmagnetic gangue minerals (i.e., calcite). The deepened color in the separated product indicated the separability of the magnetic separation. In addition, allanite-(La) was found in the separation product, as indicated by the characteristic peaks in the XRD results.

5.1.3. Summary

As outlined in Tables 4 and 5, density and magnetic separation techniques have demonstrated effectiveness in separating allanite from gangue minerals such as quartz and magnetite. Notably, the particle size of the feed is crucial in separation processes, with increased size ranges correlating with decreased separation efficiency. Moreover, achieving the appropriate degree of liberation of allanite is paramount for the success of density and magnetic separation.

Table 4
Summary of density and magnetic separation applied to complex rare-earth minerals containing allanite.

Reference	Location	Major minerals in ore feed		Particle size	SG	Magnetic field currents	Notes
[106]	India	allanite, zircon, gittinsite, aegirine, K-feldspar		< 0.5 mm	2.84, 3.32	-	Coarse-grained allanite (180–450 μm) was segregated in the fraction with SG > 3.32, while comparatively finer-sized allanite was found in the fraction with SG < 3.32, accompanied by quartz and K-feldspar.
[107]	Northern Greece	Paramagnetic	titanite, Mg-hornblende, allanite	1.70 to 0.150 mm	-	dry high-intensity magnetic separator (HIMS): 2 T with the conveyor tilt set to 72°, 74°, and 76° separately	The recovery of REEs ranged from 92% to 88%, with the REE concentration in the magnetic products being 2.8 times higher than the initial feed contents.
		Diamagnetic	albite, quartz, K-feldspar				
		Ferromagnetic	hematite, magnetite			wet HIMS: 0.48 T, 2.4 T	The allanite content increased by a factor of 2.5, from 3wt% in the initial composite feed to 8wt% in the magnetic concentrate, while the REE contents of the final magnetic concentrates increased by a factor of 2.8 compared with the initial feed.
[105]	Egypt	euxenite-(Y), fergusonite-(Y), allanite-(Ce), xenotime-(Y), uranothorite, zircon, magnetite, quartz, feldspar		1 mm to 45 μm; d_{50} = 500 μm; d_{80} = 900 μm	2.89	0.1, 1.5, 3.0 A	Allanite-(Ce) was separated into the heavy fraction (SG > 2.89) and exhibited strong paramagnetic properties that resulted in its separation at 1.5 A. The final magnetic concentrate comprised up to 63.63wt% heavy minerals with a recovery rate of 78.20%, representing a mass of 8.55% from the original sample assays containing 7.59wt% heavy minerals.

-: Not applicable.

5.2. Flotation

Flotation is a widely used method for separating valuable minerals from rock, including the beneficiation of REMs [54,108]. Currently, there is limited flotation research on allanite ore. Plaksin *et al.* [109] selected five different mineral samples to investigate the impact of the metamict character of allanite on its floatability. Sulfonated carboxylic acids (C_{16}–C_{18}) were used as collectors. The experimental findings revealed significant differences in the floatability of the four metamorphic allanite samples compared with the crystalline allanite samples. Specifically, the flotation recovery of crystalline allanite reached 90% when the collector concentration was 40 to 45 mg/L.

Jordens *et al.* [54] investigated the effect of three collectors (benzohydroxamic acid, sodium oleate, and dodecylamine) on the flotation performance of allanite and quartz. Benzohydroxamic acid and sodium oleate solutions were prepared by dissolving solids in aqueous solution, while dodecylamine was dissolved in acetic acid at a molar ratio of 1:4 and then diluted with deionized water. Sodium hydroxide and hydrochloric acid were used to adjust the pH of the solution. Quartz was ground in a rod mill and screened to obtain the fraction of 106 to 38 μm. Allanite was treated by grinding, screening, and magnetic separation to obtain the fraction of 106 to 38 μm. The zeta potentials of pure quartz and allanite were negative from pH 4 to 10, while the surface of allanite was positively charged at pH < 4. However, acid flotation is not usually preferred for industrial applications. The similar zeta potential trends of these two minerals indicate that the sorosilicate structure of allanite behaves very similarly to that of quartz. The authors suggested that separating these two minerals using collectors with adsorption mechanism solely relying on electrostatic attractive forces may be difficult. Dodecylamine may be physically absorbed on the surface of allanite through electrostatic interactions and also has significant adsorption with quartz at pH 5–10. Meanwhile, benzohydroxamic acid and sodium oleate have almost no interaction with quartz. Benzohydroxamic acid exhibits very little interaction with the allanite surface, while sodium oleate seems to overcome the inherent electrostatic repulsion and chemically absorb on the allanite surface.

Microflotation results showed that when the dosage of collectors was 200 g/t, sodium oleate and benzohydroxamic acid did not result in any flotation of quartz or allanite. Although 60% of allanite was recovered using dodecylamine, 80%–90% of quartz was also recovered, and the recovery of both minerals occurred in the first 30 s of collection. Further experiments revealed that when the dosage of dodecylamine was reduced to 20 g/t, and the pH was 7, the recovery of quartz was about 60%, while the recovery of allanite was zero, confirming the possibility of separation by reverse flotation. The authors suggested that the attraction between a cationic collector and the surface of a negatively charged mineral particle should be greater on the surface of quartz than that of allanite.

Kursun *et al.* [25] investigated the effect of ethylenediamine (CH_3–$(CH_2)_9$–O–$(CH_2)_3$–NH_2, EDA) and R845N (tetrasodium N-(1,2-dicarboxyethyl-N-octadecyl/octadecenyl sulfosuccinamate)) as collectors on the microflotation and conventional flotation performance of allanite, respectively. EDA, a collector for quartz, is an etheramine with a dodecyl radical and neutralization degree of 50% with acetic acid manufactured by Clariant. R845N, produced by Solvay Cytec, is an alkyl succinamate contained in the sulfosuccinate and sulfosuccinamate

Table 5
Summary of density and magnetic separation applied to allanite samples.

Reference	Major minerals in feed			Particle size range / μm	Magnetic field current / T	Notes
	Paramagnetic	Diamagnetic	Ferro/paramagnetic			
[8]	allanite, ankerite, fluorite	quartz, calcite, pyrite	iron oxides, other silicates	106–25	2.1, 0.45	The X-ray diffraction results showed that the primary peak of the purified allanite sample corresponded perfectly with all available allanite patterns.
[25]	allanite	calcite	-	500–212	1.66	A dry high-intensity magnetic separator under 1.66 T was used to remove nonmagnetic gangue minerals.

-: Not reported.

type collector group. Sodium silicate was used as a depressant, and methyl isobutyl carbinol was used as a frother. The researchers suggested that due to the source of the mineral specimens, composition, and structure of the mineral surfaces, the isoelectric point may vary considerably. According to the zeta potential measurements, both collectors interacted with the allanite surface in the range of pH values studied through physical adsorption. Meanwhile, contact angle measurements showed that these two collectors increased the hydrophobicity of the allanite surface in different ratios. The microflotation test results revealed that the flotation recovery of allanite increased significantly with increasing concentrations of the two collectors. Up to approximately 93% of allanite was recovered at an EDA concentration of 100 ppm, while 48.5% of allanite was recovered at an R845N concentration of 100 ppm. Moreover, the bubble-particle attachment time decreased with increasing collector concentration, and the attachment time had effects on the flotation recovery. Conventional flotation tests demonstrated that using EDA, 81.39% of allanite was recovered with a total REO grade of 0.59%, and 64.24% of allanite was recovered with a total REO grade of 0.99%, compared with the total REO grade of 0.57% in the flotation feed.

As depicted in Table 6, the studies conducted by Jordens *et al.* [54] and Kursun *et al.* [25] highlight the challenges encountered in successfully separating allanite from other silicate gangue minerals using benzohydroxamic acid, sodium oleate, dodecylamine, EDA, and R845N as collectors. As an alternative approach, it may be worthwhile to explore the reverse flotation of allanite to separate quartz. Jordens *et al.* [54] observed that at pH 7 and with a reduced dosage of dodecylamine (20 g/t), approximately 60% quartz recovery was achieved with no recovery of allanite. Furthermore, extensive flotation studies could be conducted to screen effective collectors and to investigate the synergistic effects of combining different reagents.

5.3. Leaching

Hydrometallurgy is widely recognized as one of the most economical and efficient techniques for extracting REEs from their respective ores [110,111]. REEs are typically extracted by dissolving them in a suitable leaching agent, followed by subsequent purification steps, which include solvent extraction, to refine the REEs [112].

5.3.1. Sulfuric acid roasting

Initially, allanite was treated similarly to bastnaesite, undergoing sulfuric acid roasting followed by water leaching. Moreover, concentrated hydrochloric acid is also often used to decompose allanite [113]. Historically, sulfuric acid roasting has been a major process used for REE ore processing. In this method, the REEs are converted to rare-earth sulfates, which are then dissolved in a subsequent water leach [114]. It has been demonstrated that sulfuric acid roasting at specific temperatures (200–650 °C) followed by extended water leaching (e.g., 24 h) at temperatures near boiling leads to efficient decomposition of allanite and high REE recoveries, reaching up to 95% [49,103,115–117].

However, these processes come with significant drawbacks, including high energy and equipment costs, as well as the generation of greenhouse gases and acidifying substances [49,118,119]. Therefore, recent studies have shifted focus toward direct leaching of allanite using acids or environmentally friendly electrolyte materials, similar to ionic liquids.

5.3.2. Direct leaching

Kärenlampi *et al.* [49] conducted a study on the direct leaching of allanite using sulfuric acid at room temperature, achieving approximately 80% recovery of LREEs and 60% recovery of HREEs. The raw sample obtained from Otanmäki in central Finland, consisting of allanite-(Ce), zircon, titanite, and Nb–REE–Th–U oxides, was concentrated through size reduction, hand picking, and magnetic separation. The leaching feed contained 8.1wt% of total REOs, with 7.6wt% light REOs and 0.5wt% heavy REOs, along with other main chemical compositions including SiO_2 (39.6wt%), Al_2O_3 (11.9wt%), and Fe_2O_3 (15.8wt%), as well as Th (2493 mg/kg) and U (285 mg/kg). The liquid leachate contained elevated concentrations of impurity elements such as Fe, Al, Th, Ca, and Si, which could complicate downstream processing for REE recovery. The authors investigated various leaching parameters, including leaching time, temperature, H_2SO_4 concentration, and feed particle size, while maintaining a constant solid concentration of 2%. It was found that 2 M H_2SO_4 was sufficient to dissolve REEs, with higher temperatures favoring the formation of REE sulfates, while low temperatures resulted in slower reaction rates. An optimal leaching time of 3 h was determined, as longer dissolution times led to decreased solubilities of REEs, potentially due to reprecipitation as double sulfates. Interestingly, a slightly higher recovery of REEs was observed with the coarse feed compared with the fine feed, which was attributed to passivation of the outer surfaces of allanite grains and/or REE reprecipitation effects occurring more frequently in the fine feed due to higher solubility rates. Allanite-(Ce) was identified as the dominant mineral (60wt%), although no discernible X-ray patterns from allanite-(Ce) were found, suggesting a metamict and amorphous nature of the allanite in the leaching feed. The heightened chemical reactivity of metamict allanite-(Ce) was primarily attributed to the observed low-temperature dissolution behavior.

Liu *et al.* [120] conducted direct acid leaching to recover REEs from an allanite concentrate assaying 9861.4 ppm of REEs. The effects of operational variables, such as acid type, sulfuric acid concentration, temperature, solid/liquid (S/L) ratio, and particle size, on the TREE recovery were systematically examined. The feed sample mainly consisted of albite, microcline, and actinolite, but allanite was the dominant REM in the feed sample. Other REMs in minor amounts included synchysite/bastnasite and chevkinite/tornebohmite. Acid screening tests showed that H_2SO_4 is a superior lixiviant to HNO_3 and HCl because SO_4^{2-} may act as a stronger ligand to complex with REE^{3+}.

Table 6
Summary of allanite purification through flotation.

Reference	Feed	Particle size / μm	pH	Collector		Depressant	Notes
				Type	Dosage		
[109]	crystalline and metamorphic allanite	-	-	sulfonated carboxylic acids	40–45 mg/L	-	The recovery of crystalline allanite reached 90%.
[54]	allanite sample	106–38	4, 7, 10	benzohydroxamic acid, sodium oleate, dodecylamine	20–1000 g/L	-	Quartz recovery reached 60%, while no allanite was recovered when the dosage of dodecylamine was 20 g/t, and the pH was adjusted to 7.
[25]	allanite sample	106–38	5, 7	ethylenediamine (EDA), R845N	1000–2000 g/t	sodium silicate	Flotation using EDA yielded a concentrate with a 0.59% total rare-earth element (TREE) grade and 81.39% recovery rate, while R845N resulted in a concentrate with a 0.99% TREE grade and 64.24% recovery rate, effectively doubling the TREE grade of the concentrate.

-: Not reported.

Compared with the initial H_2SO_4 concentration and particle size, temperature and S/L ratio had greater impacts on the TREE recovery during the leaching process. XRD analysis of the leaching residues indicated that the leaching process did not lead to a massive decomposition of the gangue minerals. Approximately 80% of the TREE recovery was obtained using 1 M H_2SO_4 at 75 °C for 2 h, demonstrating that most allanite could be dissolved by the acid at < 100 °C. A common leaching characteristic of the REEs is that the recovery underwent a rapid increase in the first 10 min and then slowly increased. The kinetic modeling revealed that the leaching rates of REEs at both stages were mix-controlled, i.e., a combination of both surface chemical reaction and diffusion through a product layer. Liu *et al.* [120] suggested that the initial rapid leaching rate was more likely to be explained by the preferential leaching of REMs in amorphous forms, such as metamict allanite, which was readily leachable relative to its more crystallized ones.

Karan and Sreenivas [121] studied the leaching of a rare-earth ore containing allanite using two typical choline chloride (ChCl)-based deep eutectic solvents (DESs) consisting of lactic acid and para-tolylsulfonic acid (pTSA). DES is a new class of green electrolyte materials with environmental benignity. They found that approximately 95% of REEs could be leached using ChCl : pTSA at a 1:1 molar ratio, with a 6 h reaction time at 130 °C and a liquid-to-solid weight ratio of 10. Subsequently, approximately 98% of the dissolved REEs could be precipitated as REE fluoride, which was 85% pure. Their studies with DES also highlighted the critical role of medium viscosity and reaction temperature on the efficiency of REE leachability. The raw ore was sourced from a microgranite-type hard rock deposit in Bhatikhera, Rajasthan, with an assay of approximately 0.36% REEs, with approximately 40% comprising HREEs. The REE-carrying phases were identified as allanite, gittinsite, and zircon, with REO contents of 19.7wt%, 2.1wt%, and 0.74wt%, respectively. The major gangue minerals included aegirine ($NaFeSi_2O_6$), quartz, and K-feldspar. The ore also contained SiO_2 (40.4wt%), Fe_2O_3 (8.6wt%), Al_2O_3 (7.2wt%), K_2O (4.4wt%), Na_2O (4.4wt%), CaO (1.2wt%), and Zr (0.66wt%), with a low Th content of only 0.01wt%. The presence of low radioactive elements minimized the environmental burden and reduced the number of stages in the process scheme. Comparison of DES performance with conventionally used direct mineral acids and sulfation roasting and aqueous leaching alternatives indicated the superiority of DES not only in terms of leach recovery but also in selectivity.

5.3.3. Summary

As illustrated in Table 7, the results from the literature demonstrate the feasibility of directly leaching REEs from metamict allanite using sulfuric acid. Allanite has also been shown to be soluble in DES. However, it is worth noting that the reports do not address the issue of silica gel formation during leaching despite the high silica content of allanite. Furthermore, a significant number of impurity metals, such as Fe, Al, and Ca, are co-dissolved and need to be removed in subsequent purification steps. Some allanite leach solutions exhibit an excess of thorium, which requires timely removal. Indeed, there is still a notable gap in systematic studies regarding allanite leaching, largely due to the compositional variations among different allanite samples.

5.4. Envisioning future research trajectories

Table 8 provides an overview of the current research on allanite processing and outlines potential directions for future research on allanite by drawing insights from technologies applied to other REMs. Currently, the processing sequence for allanite begins with physical separation (i.e., crushing, sieving, density separation, magnetic separation, flotation) followed by leaching to extract the REEs into the leach solution. This solution is then utilized in the subsequent production route for refining rare-earth products.

The efficiency of enriching allanite through physical crushing, sieving, and combining density and magnetic separation has been validated in laboratory settings, effectively eliminating gangue minerals such as quartz and magnetite. Notably, achieving optimal separation efficiency relies on two pivotal factors: ensuring proper liberation of allanite through the crushing and grinding process and segregating the feed into distinct particle size fractions, each subjected to corresponding gravity and magnetic separation conditions.

Flotation encounters challenges when it comes to separating allanite from other silicate gangue minerals. Current research on a restricted range of flotation collector types has resulted in unsatisfactory separation outcomes. However, an area worthy of further investigation is the potential for reverse flotation using dodecylamine as a collector through dosage adjustment. Future research on allanite flotation will require comprehensive screening of effective collectors and exploration of the synergistic effects of different reagent combinations, which will entail extensive experimental work.

In terms of leaching, the traditional approach has been to apply monazite processing methods to allanite, involving sulfuric acid roasting and water leaching. Recent research has shifted focus toward direct acid leaching of allanite. One significant finding is that the ease of allanite leaching is related to its crystallinity. As allanite typically contains radioactive thorium and uranium elements, some allanite may transform into less crystalline metamict allanite during alteration process. Meanwhile, the leaching of thorium and uranium during the

Table 7
Summary of direct leaching studies on allanite.

Reference	Feed	Particle size	Solid/liquid ratio	Lixiviant	Temperature / °C	Time / h	Recovery
[49]	allanite concentrate	d_{50} = 327 μm	100/2000 g/mL	2 M H_2SO_4	22	3	80% of light REEs and 60% of heavy REEs
[120]	allanite concentrate	d_{80} = 47.9 μm	25 g/L	1 M H_2SO_4	75	2	80% of total REEs
[121]	allanite ore	mesh of grind < 400#	1:10	ChCl : pTSA (1:1)	130	6	95% of REEs

Table 8
Summary of the present studies on allanite processing, along with suggestions for potential future research directions.

Processing steps	Feed	Processing technologies		Notes
Physical beneficiation	allanite	liberation sieving density separation magnetic separation		Effective, but the key lies in the liberation of allanite and the range of particle sizes.
		froth flotation		Challenging, but enrichment through reverse flotation may be possible. Future research will necessitate thorough screening of effective collectors and exploration of the synergistic effects of different reagent combinations.
Leaching	metamict allanite	direct acid leaching		Allanite can be leached in multiple steps. For poorly crystalline metamict allanite, direct acid leaching is suitable. For well-crystallized, difficult-to-leach allanite, future research may focus on auxiliary leaching and enhanced leaching.
	crystalline allanite	auxiliary/ enhanced leaching	acid roasting alkaline bioleaching ultrasound electrochemical microwave autoclave others	
Purification	rare-earth elements	solvent extraction selective precipitation selective adsorption membrane separation others		Extensive research has been conducted to date.

alteration process leads to a reduction in the concentration of radioactive elements. Therefore, metamict allanite can be leached directly with acid. Due to variations in the origin of allanite deposits and the influence of upstream processing, there can be significant differences in the mineral composition and crystallinity of allanite used for leaching. Hence, allanite can be leached in multiple steps. For poorly crystalline allanite, direct acid leaching is suitable, and future research directions may focus on optimizing leaching conditions and studying kinetics. For well-crystallized, difficult-to-leach allanite, future research may focus on auxiliary leaching and enhanced leaching, including alkaline leaching, bioleaching, ultrasound leaching, electrochemical leaching, microwave leaching, and autoclave leaching.

6. Conclusions

Allanite is commonly encountered as an accessory rare-earth silicate mineral in association with minerals such as garnet, biotite, and feldspar. It is distributed globally and occurs in igneous formations such as granite, pegmatite, and syenite, as well as in various metamorphic rocks such as schist, gneiss, and amphibolite. Moreover, it can be found in mineral veins formed through hydrothermal activity. The presence of radioactive elements such as uranium and thorium in allanite can lead to alteration processes. Its appearance and texture can vary considerably based on the specific metamorphic reactions it has experienced. Furthermore, allanite emerges as a valuable tool for geochronological analysis for the precise delineation of geological events.

While allanite has not yet been extensively utilized for the production of REEs, recent discoveries of high-grade rare-earth-rich allanite deposits in Wyoming in the United States highlight its economic potential. Given the concerns about scarcity and potential global shortages of rare earths, there is increasing interest in exploring alternative sources such as allanite. However, despite ongoing research on the mineralogy and processing of rare-earth metals, allanite has not received widespread attention in mineral processing.

Currently, research has shown that density and magnetic separation techniques are effective methods for separating allanite from gangue minerals such as quartz and magnetite. However, flotation studies have faced challenges in separating allanite from other silicate gangue minerals. Various collectors, including benzohydroxamic acid, sodium oleate, dodecylamine, EDA, and R845N, have been tested to investigate REE recovery, but achieving effective separation remains difficult. As an alternative approach, exploring the reverse flotation of allanite to separate quartz could be worthwhile. Moreover, extensive flotation studies could be conducted to screen for effective collectors and investigate the synergistic effects of combining different reagents. As for leaching, the ease of allanite leaching is related to its crystallinity. Hence, allanite can be leached in multiple steps. For poorly crystalline allanite, direct acid leaching is suitable. For well-crystallized, difficult-to-leach allanite, future research may focus on auxiliary leaching and enhanced leaching, including alkaline leaching, bioleaching, ultrasound leaching, electrochemical leaching, microwave leaching, and autoclave leaching. Meanwhile, some allanite leach solutions could exhibit an excess of thorium, which requires timely removal. In conclusion, to achieve cost-effective production of REEs from allanite in the future, systematic studies on processing techniques are imperative to fully unlock the potential of allanite as an REE source.

CRediT authorship contribution statement

Zhongqing Xiao: Conceptualization, Investigation, Visualization, Writing – original draft. **Wencai Zhang**: Writing – review & editing, Supervision, Project administration, Funding acquisition.

Declaration of Competing Interest

Wencai Zhang is an editorial board member for this journal and was not involved in the editorial review or the decision to publish this article. The authors declare the following financial interests/personal relationships which may be considered as potential competing interests: Wencai Zhang reports financial support was provided by US Department of Energy.

Acknowledgements

This material is based upon work supported by the U.S. Department of Energy's Office of Energy Efficiency and Renewable Energy (EERE) under the Advanced Manufacturing Office Award Number DE-EE0009435. Phinix, LLC is the primary recipient of this award.

References

[1] N. Dushyantha, N. Batapola, I.M.S.K. Ilankoon, S. Rohitha, R. Premasiri, B. Abeysinghe, N. Ratnayake, K. Dissanayake, The story of rare earth elements (REEs): Occurrences, global distribution, genesis, geology, mineralogy and global production, Ore Geol. Rev. 122 (2020) 103521.
[2] B.S. Van Gosen, P.L. Verplanck, K.R. Long, J. Gambogi, R.R. Seal, The rare-earth elements: Vital to modern technologies and lifestyles, in: Fact Sheet 2014–3078, U. S. Geological Survey, Reston, 2014.
[3] V. Fernandez, Rare-earth elements market: A historical and financial perspective, Resour. Policy 53 (2017) 26–45.
[4] R.L. Rudnick, S. Gao, 3.01 Composition of the continental crust, in: H.D. Holland, K.K. Turekian (Eds.), Treatise on Geochemistry, Elsevier, Amsterdam, 2003, pp. 1–64.
[5] V.T. McLemore, Rare earth elements (REE) deposits in New Mexico: Update, New Mex. Geol. 37 (3) (2015) 59–69.
[6] G.B. Haxel, J.B. Hedrick, G.J. Orris, Rare earth elements: Critical resources for high technology, in: Fact Sheet 087–02, U.S. Geological Survey, Reston, 2002.
[7] A.V. Naumov, Review of the world market of rare-earth metals, Russ. J. Non-Ferr. Met. 49 (1) (2008) 14–22.
[8] A. Jordens, Y.P. Cheng, K.E. Waters, A review of the beneficiation of rare earth element bearing minerals, Miner. Eng. 41 (2013) 97–114.
[9] S. Vijayan, A.J. Melnyk, R.D. Singh, K. Nuttall, Rare earths, Min. Eng. 41 (1) (1989) 13–20.
[10] R.A. Chi, S.M. Xu, G.C. Zhu, J.M. Xu, X. Qiu, Benefication of rare earth ore in China, in: Light Metals: Proceedings of Sessions, TMS Annual Meeting, Warrendale, 2001, pp. 1159–1165.
[11] B.K. Gupta, M. Lal, S.C. Sharma, Improving quality of service parameters in wireless asynchronous transfer mode network, in: IEE Mobility Conference 2005, The Second International Conference on Mobile Technology, Applications and Systems, Guangzhou, 2005.
[12] C.K. Gupta, N. Krishnamurthy, Extractive metallurgy of rare earths, Int. Mater. Rev. 37 (1) (1992) 197–248.
[13] A.R. Jha, Rare Earth Materials: Properties and Applications, CRC Press, Boca Raton, 2014.
[14] B. Deng, X. Wang, D.X. Luong, R.A. Carter, Z. Wang, M.B. Tomson, J.M. Tour, Rare earth elements from waste, Sci. Adv. 8 (6) (2022) eabm3132.
[15] V. Balaram, Potential future alternative resources for rare earth elements: Opportunities and challenges, Minerals 13 (3) (2023) 425.
[16] Y. Kanazawa, M. Kamitani, Rare earth minerals and resources in the world, J. Alloy. Compd. 408-412 (2006) 1339–1343.
[17] N. Haque, A. Hughes, S. Lim, C. Vernon, Rare earth elements: Overview of mining, mineralogy, uses, sustainability and environmental impact, Resources 3 (4) (2014) 614–635.
[18] B.L. Zhou, Z.X. Li, C.C. Chen, Global potential of rare earth resources and rare earth demand from clean technologies, Minerals 7 (11) (2017) 203.
[19] Y.X. Ni, J.M. Hughes, A.N. Mariano, The atomic arrangement of bastnäesite-(Ce), $Ce(CO_3)F$, and structural elements of synchysite-(Ce), röntgenite-(Ce), and parisite-(Ce), Am. Miner. 78 (3-4) (1993) 415–418.
[20] X.S. Yang, J.V. Satur, K. Sanematsu, J. Laukkanen, T. Saastamoinen, Beneficiation studies of a complex REE ore, Miner. Eng. 71 (2015) 55–64.
[21] C.J. Ferron, S.M. Bulatovic, R.S. Salter, Beneficiation of rare earth oxide minerals, Mater. Sci. Forum 70-72 (1991) 251–270.
[22] E.H. Oelkers, F. Poitrasson, An experimental study of the dissolution stoichiometry and rates of a natural monazite as a function of temperature from 50 to 230°C and pH from 1.5 to 10, Chem. Geol. 191 (1-3) (2002) 73–87.
[23] Y. Hikichi, T. Ota, K. Daimon, T. Hattori, M. Mizuno, Thermal, mechanical, and chemical properties of sintered xenotime-type RPO_4 (R = Y, Er, Yb, or Lu), J. Am. Ceram. Soc. 81 (8) (1998) 2216–2218.
[24] S.C. Chelgani, M. Rudolph, T. Leistner, J. Gutzmer, U.A. Peuker, A review of rare earth minerals flotation: Monazite and xenotime, Int. J. Min. Sci. Technol. 25 (6) (2015) 877–883.
[25] I. Kursun, M. Terzi, O. Ozdemir, Determination of surface chemistry and flotation properties of rare earth mineral allanite, Miner. Eng. 132 (2019) 113–120.
[26] G.A. Moldoveanu, V.G. Papangelakis, Recovery of rare earth elements adsorbed on clay minerals: I. Desorption mechanism, Hydrometallurgy, 117- 118 (2012) 71–78.
[27] M.F. Zhou, M.Y.H. Li, Z.C. Wang, X.C. Li, J.C. Liu, The genesis of regolith-hosted rare earth element and scandium deposits: Current understanding and outlook to future prospecting, Chin. Sci. Bull. 65 (33) (2020) 3809–3824.
[28] X. Feng, O. Onel, M. Council-Troche, A. Noble, R.H. Yoon, J.R. Morris, A study of rare earth ion-adsorption clays: The speciation of rare earth elements on kaolinite at basic pH, Appl. Clay Sci. 201 (2021) 105920.
[29] Z.X. Wu, Y. Chen, Y. Wang, Y. Xu, Z.L. Lin, X.L. Liang, H.F. Cheng, Review of rare earth element (REE) adsorption on and desorption from clay minerals: Application to formation and mining of ion-adsorption REE deposits, Ore Geol. Rev. 157 (2023) 105446.
[30] M. Aide, C. Aide, Rare earth elements: Their importance in understanding soil genesis, Int. Sch. Res. Not. 2012 (2012) 1–11.
[31] M. Hoshino, K. Sanematsu, Y. Watanabe, Chapter 279—REE mineralogy and resources, in: Handbook on the Physics and Chemistry of Rare Earths, Elsevier, Amsterdam, 2016, pp. 129–291.
[32] R.D. Shannon, Revised effective ionic radii and systematic studies of interatomic distances in halides and chalcogenides, Acta Crystallogr. Sect. A 32 (5) (1976) 751–767.
[33] V. Balaram, Rare earth elements: A review of applications, occurrence, exploration, analysis, recycling, and environmental impact, Geosci. Front. 10 (4) (2019) 1285–1303.
[34] S. Massari, M. Ruberti, Rare earth elements as critical raw materials: Focus on international markets and future strategies, Resour. Policy 38 (1) (2013) 36–43.
[35] K.M. Goodenough, F. Wall, D. Merriman, The rare earth elements: Demand, global resources, and challenges for resourcing future generations, Nat. Resour. Res. 27 (2) (2018) 201–216.
[36] W.C. Zhang, A. Noble, X.B. Yang, R. Honaker, A comprehensive review of rare earth elements recovery from coal-related materials, Minerals 10 (5) (2020) 451.
[37] D.A. Atwood, The Rare Earth Elements: Fundamentals and Applications, John Wiley & Sons, 2013.
[38] S. Peelman, D. Kooijman, J. Sietsma, Y. Yang, Hydrometallurgical recovery of rare earth elements from mine tailings and WEEE, J. Sustain. Metall. 4 (3) (2018) 367–377.
[39] C.R. Borra, Y. Pontikes, K. Binnemans, T. Van Gerven, Leaching of rare earths from bauxite residue (red mud), Miner. Eng. 76 (2015) 20–27.
[40] V.N. Rychkov, E.V. Kirillov, S.V. Kirillov, V.S. Semenishchev, G.M. Bunkov, M.S. Botalov, D.V. Smyshlyaev, A.S. Malyshev, Recovery of rare earth elements from phosphogypsum, J. Clean. Prod. 196 (2018) 674–681.
[41] P.N. Gamaletsos, A. Godelitsas, A. Filippidis, Y. Pontikes, The rare earth elements potential of Greek bauxite active mines in the light of a sustainable REE demand, J. Sustain. Metall. 5 (1) (2019) 20–47.
[42] K. Binnemans, P.T. Jones, B. Blanpain, T. Van Gerven, Y.X. Yang, A. Walton, M. Buchert, Recycling of rare earths: A critical review, J. Clean. Prod. 51 (2013) 1–22.
[43] L. Peter Gromet, L.T. Silver, Rare earth element distributions among minerals in a granodiorite and their petrogenetic implications, Geochim. Cosmochim. Acta 47 (5) (1983) 925–939.
[44] W.N. Sawka, B.W. Chappell, K. Norrish, Light-rare-earth-element zoning in sphene and allanite during granitoid fractionation, Geology 12 (3) (1984) 131.
[45] D.A. Carswell, R.N. Wilson, M. Zhai, Metamorphic evolution, mineral chemistry and thermobarometry of schists and orthogneisses hosting ultra-high pressure eclogites in the Dabieshan of central China, Lithos 52 (1) (2000) 121–155.
[46] S.S. Sorensen, Petrogenetic significance of zoned allanite in garnet amphibolites from a paleo-subduction zone: Catalina Schist, southern California, Am. Mineral. 76 (3-4) (1991) 589–601.
[47] R. Tribuzio, B. Messiga, R. Vannucci, P. Bottazzi, Rare earth element redistribution during high-pressure–low-temperature metamorphism in ophiolitic Fe-gabbros (Liguria, northwestern Italy): Implications for light REE mobility in subduction zones, Geology 24 (8) (1996) 711.
[48] G.D. Gatta, F. Pagliaro, P. Lotti, A. Guastoni, L. Cañadillas-Delgado, O. Fabelo, L. Gigli, Allanite at high temperature: Effect of REE on the thermal behaviour of epidote-group minerals, Phys. Chem. Miner. 48 (9) (2021) 32.
[49] K. Kärenlampi, E. Väänänen, T. Roivainen, P. Perämäki, Low temperature leaching behavior of allanite-(Ce) in treating an allanite-concentrate by sulfuric acid, J. Sustain. Metall. 10 (1) (2024) 771.
[50] American Rare Earths, Proactive: American Rare Earths stakes new high-grade deposit in Wyoming, American Rare Earths, 2023. 〈https://americanrareearths.com.au/proactive-american-rare-earths-stakes-new-high-grade-deposit-in-wyoming-us/〉 (Accessed January 1, 2024).
[51] R. Giere, S.S. Sorensen, Allanite and other REE-rich epidote-group minerals, Rev. Mineral. Geochem. 56 (1) (2004) 431–493.
[52] T.S. Ercit, The mess that is "allanite", Can. Mineral. 40 (5) (2002) 1411–1419.
[53] V.I. Sachkov, R.A. Nefedov, R.O. Medvedev, I.V. Amelichkin, A.S. Sachkova, P.S. Shcherbakov, V.S. Solovyev, D.I. Leonov, D.A. Biryukov, Content and forms of radioactive elements in orthite (allanite), Minerals 13 (3) (2023) 366.
[54] A. Jordens, C. Marion, O. Kuzmina, K.E. Waters, Physicochemical aspects of allanite flotation, J. Rare Earths 32 (5) (2014) 476–486.
[55] K.J. Murata, H.J. Rose Jr, M.K. Carron, J.J. Glass, Systematic variation of rare-earth elements in cerium-earth minerals, Geochim. Cosmochim. Acta 11 (3) (1957) 141–161.
[56] V.A. Khvostova, Mineralogy of orthite, Institut mineralogii, geokhimii, i kristallokhimii redkikh elementov, Akad. Nauk SSSR, Tr. 11 (1962) 119.
[57] A.A. Levinson, A system of nomenclature for rare-earth minerals, Am. Mineral. 51 (1966) 152–158.

[58] E.H. Nickel, A.J. Naldrett, Procedures Involving the IMA Commission On New Minerals and Mineral Names. and guidelines on mineral nomenclature, Can. Mineral. 25 (2) (1987) 353–377.
[59] V. Khvostova, Isomorphism of epidote and orthite, Akad. Nauk SSSR, Dokl. 141 (6) (1961) 1461.
[60] V.V. Ploshko, V.I. Bogdanova, Isomorphous substitutions in minerals of the epidote group from the northern Caucasus, Geochemistry 1 (1963) 61–71.
[61] H.G. Tempel, Der Einfluss der seltenen Erden und einiger anderer Komponenten auf die physikalisch-optischen Eigenschaften innerhalb der Epidotgruppe (The influence of rare earths and some other components on the physico-optical properties within the epidote group), Chem. der Erde 11 (4) (1938) 525–551.
[62] W.D. Nesse, Introduction to Optical Mineralogy, 3rd ed., Oxford University Press, London, 2003.
[63] G. Franz, A. Liebscher, Physical and chemical properties of the epidote minerals—An introduction, Rev. Mineral. Geochem. 56 (1) (2004) 1–81.
[64] C.D. Gribble, Rutley's Elements of Mineralogy, Springer, Dordrecht, 1988.
[65] S.I. Arbuzov, A.V. Volostnov, L.P. Rikhvanov, A.M. Mezhibor, S.S. Ilenok, Geochemistry of radioactive elements (U,Th) in coal and peat of northern Asia (Siberia, Russian Far East, Kazakhstan, and Mongolia), Int. J. Coal Geol. 86 (4) (2011) 318–328.
[66] H.H. Guo, Y.L. Xiao, L.J. Xu, H. Sun, J. Huang, Z.H. Hou, Origin of allanite in gneiss and granite in the Dabie orogenic belt, Central East China, J. Asian Earth Sci. 135 (2017) 243–256.
[67] A.J. Smye, N.M.W. Roberts, D.J. Condon, M.S.A. Horstwood, R.R. Parrish, Characterising the U–Th–Pb systematics of allanite by ID and LA-ICPMS: Implications for geochronology, Geochim. Cosmochim. Acta 135 (2014) 1–28.
[68] J.A. Vazquez, M.R. Reid, Probing the accumulation history of the voluminous toba magma, Science 305 (5686) (2004) 991–994.
[69] A.D. Burnham, R. Chandler, Y. Amelin, J. Mavrogenes, Allanite geochronology in the Mount Isa Inlier, Aust. J. Earth Sci. (2023), https://doi.org/10.1080/08120099.2023.2291514.
[70] A.E. Abdel Gawad, K. Ali, H. Eliwa, M.I. Sayyed, M.U. Khandaker, D.A. Bradley, H. Osman, B.H. Elesawy, M.Y. Hanfi, Radiological investigation on sediments: A case study of wadi rod elsayalla the southeastern desert of Egypt, Appl. Sci. 11 (24) (2021) 11884.
[71] J. Janeczek, R.K. Eby, Annealing of radiation damage in allanite and gadolinite, Phys. Chem. Miner. 19 (6) (1993) 343–356.
[72] R.C. Ewing, A. Meldrum, L. Wang, S. Wang, Radiation-induced amorphization, Rev. Mineral. Geochem. 39 (1) (2000) 319–361.
[73] C.E. Reissner, U. Bismayer, D. Kern, M. Reissner, S. Park, J.M. Zhang, R.C. Ewing, A. Shelyug, A. Navrotsky, C. Paulmann, R. Škoda, L.A. Groat, H. Pöllmann, T. Beirau, Mechanical and structural properties of radiation-damaged allanite-(Ce) and the effects of thermal annealing, Phys. Chem. Miner. 46 (10) (2019) 921–933.
[74] T. Beirau, Annealing Induced Recrystallization of Radiation Damaged Titanite and Allanite (Dissertation), Universität Hamburg, Hamburg, Germany, 2012.
[75] J.R. Price, D.H.C. Wilton, M.N. Tubrett, J.S. Schneiderman, X.D. Fan, K. Peresolak, Predicting radioactive accessory mineral dissolution during chemical weathering: The radiation dose at the solubility threshold for epidote-group detrital grains from the Yangtze River Delta, China, Chem. Geol. 393- 394 (2015) 93–111.
[76] M. Zhang, Raman study of the crystalline-to-amorphous state in alpha-decay–-damaged materials, in: M. Khan (Ed.), Raman Spectroscopy and Applications, InTechOpen, Rijeka, 2017.
[77] T. Beirau, C. Paulmann, U. Bismayer, Recrystallization of metamict allanite, Mineral. Mag. 75 (4) (2011) 2393–2399.
[78] C.E. Reissner, M. Reissner, D. Kern, H. Pöllmann, T. Beirau, Iron sites in radiation-damaged allanite-(Ce): The effects of thermally induced oxidation and structural reorganization, Hyperfine Inter. 241 (1) (2020) 18.
[79] D.C. Pal, A. Banerjee, A. Dutta, A.K. Sarangi, Hydrothermal alterations and U-REE mineralisation in the Narwapahar uranium deposit, Singhbhum shear zone, India, J. Earth Syst. Sci. 131 (1) (2022) 31.
[80] S.Abu Elatta Abdallah Mahmoud, Geology, mineralogy and mineral chemistry of the NYF-type pegmatites at the Gabal El Faliq Area, South Eastern Desert, Egypt, J. Earth Syst. Sci. 128 (6) (2019) 156.
[81] D.A. Mineev, Lantanoidy v mineralakh: (Stat. Issledovanie otnosit rasprostranennosti i raspredeleiiia) (Lanthanoids in Minerals: Statistical Study on Distribution and Dispersion), Nedra, Moskva, 1969 (in Russian).
[82] E. Semenov, Orudenenie i mineralizacija redkich zemel, torija i urana (lantanidov i aktinidov) (Ore Formation and Mineralization of Rare Earths, Thorium, and Uranium (Lanthanides and Actinides)), Moscow, 2001 (in Russian).
[83] C.M. Gramaccioli, Die Mineralien der Alpen: eine Übersicht über die aus dem Alpenraum bekannten Mineralien; mit einer Einführung in Mineralogie und Kristallographie (The Minerals of the Alps: An Overview of the Minerals Known from the Alpine Region; with an Introduction to Mineralogy and Crystallography), Franckh, 1978 (in German).
[84] A.N. Labuntsov, Pegmatites of the North Karelia, Pegmatity SSSR, Akad. Nauk SSSR, Moscow-Leningrad, 1939.
[85] K.K. Zhirov, Geochemistry of rare-earth elements in pegmatites of north Karelia, Geochemistry 11 (1961) 995–1004.
[86] C.J. Gregory, D. Rubatto, J. Hermann, A. Berger, M. Engi, Allanite behaviour during incipient melting in the southern Central Alps, Geochim. Cosmochim. Acta 84 (2012) 433–458.
[87] E.V. Putintseva, E.M. Spiridonov, Allanite-(Ce): A typical mineral of meta-kimberlite from the lake kimozero area, Karelia, Geol. Ore Depos. 59 (8) (2017) 720–728.
[88] F. Finger, I. Broska, M.P. Roberts, A. Schermaier, Replacement of primary monazite by apatite–allanite–epidote coronas in an amphibolite facies granite gneiss from the Eastern Alps, Am. Mineral. 83 (3-4) (1998) 248–258.
[89] E. Janots, M. Engi, A. Berger, J. Allaz, J.O. Schwarz, C. Spandler, Prograde metamorphic sequence of REE minerals in pelitic rocks of the Central Alps: implications for allanite–monazite–xenotime phase relations from 250 to 610°C, J. Metamorph. Geol. 26 (5) (2008) 509–526.
[90] E. Janots, A. Berger, M. Engi, Physico–chemical control on the REE minerals in chloritoid-grade metasediments from a single outcrop (Central Alps, Switzerland), Lithos 121 (1-4) (2011) 1–11.
[91] L. Airaghi, E. Janots, P. Lanari, J. de Sigoyer, V. Magnin, Allanite petrochronology in fresh and retrogressed garnet–biotite metapelites from the Longmen Shan (Eastern Tibet), J. Petrol. 60 (1) (2019) 151–176.
[92] S. Vlach, G. Gualda, Allanite and chevkinite in A-type granites and syenites of the Graciosa Province, southern Brazil, Lithos 97 (1-2) (2007) 98–121.
[93] V.R. Akhila, S. Rakesh, S.C. Gupta, A. Mukherjee, D. Bhattacharya, K. Chakrabarti, D.K. Sinha, Allanite in singhbhum shear zone, India and its implications on the genesis of REE mineralization, J. Geol. Soc. Ind. 98 (8) (2022) 1042–1050.
[94] I. Broska, I. Petrík, C.T. Williams, Coexisting monazite and allanite in peraluminous granitoids of the Tribeč Mountains, Western Carpathians, Am. Mineral. 85 (1) (2000) 22–32.
[95] Y. Kim, K. Yi, M. Cho, Parageneses and Th–U distributions among allanite, monazite, and xenotime in Barrovian-type metapelites, Imjingang belt, central Korea, Am. Mineral. 94 (4) (2009) 430–438.
[96] B.A. Wing, J.M. Ferry, T.M. Harrison, Prograde destruction and formation of monazite and allanite during contact and regional metamorphism of pelites: Petrology and geochronology, Contrib. Mineral. Petrol. 145 (2) (2003) 228–250.
[97] S.L. Corrie, M.J. Kohn, Trace-element distributions in silicates during prograde metamorphic reactions: Implications for monazite formation, J. Metamorph. Geol. 26 (4) (2008) 451–464.
[98] A. Cavallo, G.A. Dino, Extractive waste as a resource: Quartz, feldspars, and rare earth elements from gneiss quarries of the Verbano-Cusio-Ossola Province (Piedmont, northern Italy), Sustainability 14 (8) (2022) 4536.
[99] X. Zhao, N.B. Li, H.C. Niu, Y.H. Jiang, S. Yan, Y.Y. Yang, R.X. Fu, Hydrothermal alteration of allanite promotes the generation of ion-adsorption LREE deposits in South China, Ore Geol. Rev. 155 (2023) 105377.
[100] S.L. Hanson, A.U. Falster, W.B. Simmons, T.A. Brown, Allanite-(Nd) from the Kingman feldspar mine, Mojave pegmatite district, northwestern Arizona, USA, Can. Mineral. 50 (4) (2012) 815–824.
[101] M.K. Jha, A. Kumari, R. Panda, J. Rajesh Kumar, K. Yoo, J.Y. Lee, Review on hydrometallurgical recovery of rare earth metals, Hydrometallurgy 165 (2016) 2–26.
[102] F. Sadri, A.M. Nazari, A. Ghahreman, A review on the cracking, baking and leaching processes of rare earth element concentrates, J. Rare Earths 35 (8) (2017) 739–752.
[103] D. Dreisinger, G. Andrews, N. Verbaan, M. Johnson, E. Bourricaudy, The demonstration pilot plant results for the search minerals direction extraction process for rare earth recovery, Rare Metal Technology 2018, TMS Annual Meeting & Exhibition, Springer, Cham, 2018, pp. 3–14.
[104] D. Dreisinger, Rare-earth and critical material recovery from peralkaline volcanic ores: Minerals processing, hydrometallurgy, and solvent extraction separation, Rare Metal Technology 2022, Springer, Cham, 2022, pp. 3–16.
[105] M.F. Raslan, S. Kharbish, M.M. Fawzy, M.M. El Dabe, M.M. Fathy, Gravity and magnetic separation of polymetallic pegmatite from wadi el sheih granite, central eastern desert, Egypt, J. Min. Sci. 57 (2) (2021) 316–326.
[106] R. Karan, T. Sreenivas, J.M. Babu, M.A. Kumar, K.A. Rao, H.S. Sahoo, A. Banerjee, K.L. Mundra, Hydrometallurgical studies for the recovery of rare earths from micro-granite ore deposit of Bhatikhera, Rajasthan, India, J. Geol. Soc. Ind. 98 (8) (2022) 1152–1158.
[107] C. Stouraiti, V. Angelatou, S. Petushok, K. Soukis, D. Eliopoulos, Effect of mineralogy on the beneficiation of REE from heavy mineral sands: The case of Nea Peramos, Kavala, northern Greece, Minerals 10 (5) (2020) 387.
[108] A.V. Nguyen, FLOTATION, in: I.D. Wilson (Ed.), Encyclopedia of Separation Science, Academic Press, Oxford, 2007, pp. 1–27.
[109] I.N. Plaksin, K.F. Barysheva, V.I. Solnyshkin, V.A. Khvostova, Effect of metamict decomposition of orthite on its floatability, Sov. Min. Sci. 6 (4) (1970) 412–416.
[110] F. Habashi, Handbook of Extractive Metallurgy Volume 3, Wiley-VCH, 1997.
[111] F. Habashi, Extractive metallurgy of rare earths, Can. Metall. Q. 52 (3) (2013) 224–233.
[112] A. Shahbaz, A systematic review on leaching of rare earth metals from primary and secondary sources, Miner. Eng. 184 (2022) 107632.
[113] J. Zhang, C. Edwards, Mineral decomposition and leaching processes for treating rare earth ore concentrates, Can. Metall. Q. 52 (3) (2013) 243–248.
[114] J. Demol, E. Ho, K. Soldenhoff, G. Senanayake, The sulfuric acid bake and leach route for processing of rare earth ores and concentrates: A review, Hydrometallurgy 188 (2019) 123–139.
[115] D. Dreisinger, N. Verbaan, M. Johnson, The search minerals direct extraction process for rare earth element recovery, Rare Metal Technology 2016, Springer, Cham, 2016, pp. 3–16.

[116] D. Dreisinger, N. Verbaan, M. Johnson, The Processing of REE's from Search Minerals' Foxtrot Resource—An Update, Canadian Institute of Mining, Metall. Pet. (2014) 81–94.
[117] M.G. Baillie, J.D. Hayton, A process for the recovery of high grade rare earth concentrates from Mary Kathleen uranium tailings, in: 9th International Mineral Processing Congress, Institution of Mining and Metallurgy, London, Prague, Czechoslovakia, 1970, pp. 334–345.
[118] L. Talens Peiró, G. Villalba Méndez, Material and energy requirement for rare earth production, JOM 65 (10) (2013) 1327–1340.
[119] M. Jouini, A. Royer-Lavallée, T. Pabst, E. Chung, R. Kim, Y.W. Cheong, C.M. Neculita, Sustainable production of rare earth elements from mine waste and geoethics, Minerals 12 (7) (2022) 809.
[120] W. Liu, Z.Q. Xiao, S. Das, W.C. Zhang, Mechanism and kinetic study of rare earth extraction from allanite by direct acid leaching, Miner. Eng. 205 (2024) 108489.
[121] R. Karan, T. Sreenivas, Recovery of rare earth values from micro-granite type hard rocks using deep eutectic solvents, Trans. Indian Inst. Met. (2023), https://doi.org/10.1007/s12666-023-02946-w.